

Design of a 4×8 Substrate Integrated Waveguide Butler Matrix with Sidelobe Suppression at 60 GHz

Zahra Mehrzad

Department of Electrical
Engineering
AmirKabir University of
Technology
Tehran, Iran
s.mehrzad@aut.ac.ir

Gholamreza Moradi*

Department of Electrical Engineering AmirKabir University of Technology Tehran, Iran ghmoradi@aut.ac.ir

Ayaz Ghorbani

Department of Electrical Engineering AmirKabir University of Technology Tehran, Iran ghorbani@aut.ac.ir

Received: 8 January 2021 - Accepted: 11 March 2021

Abstract—This article presents a novel 4×8 SIW Butler matrix (BM) with sidelobe level (SLL) suppression. The BM operates at 60 GHz and is implemented with a new design to achieve a compact size, which would be attractive for future mmWave wireless systems. This beamforming network uses straight SIW phase shifters with two apertures or two metal posts to pursue a smaller circuit area than with curved line phase shifters. Using a stepwise procedure and analyzing the design equations, the crossover and other components of the BM are also designed and optimized. The reflection and isolation coefficients are lower than -10 dB for all input ports and insertion loss magnitude imbalance is below 2.4 dB within the band from 57 GHz to 67 GHz. The slot array antenna fed by the BM shows an SLL lower than -21 dB for inputs 1 and 4 and lower than -14.5 dB for inputs 2 and 3 and provides $\pm45^{\circ}$ beam switching.

 $\label{lem:keywords} \textbf{\textit{Keywords}--Beamforming network (BFN); 4} \textbf{\textit{x}} \textbf{\textit{8} Butler matrix; Substrate Integrated Waveguide (SIW); Sidelobe level (SLL); millimeter-wave}$

I. INTRODUCTION

Increasing users' demand for new services, data traffic growth, and the increase in the number of devices connected to wireless networks have necessitated the development of existing networks, and the need for a wider frequency spectrum has increased. Therefore, many researchers have shifted the focus of their studies to the idea of networks beyond the fourth-generation or the fifth-generation networks (5G technology) as well as the millimeter-wave frequency range (30 GHz-300 GHz) [1,2]. The 60 GHz band has become a very suitable choice for short-range communications and

WLAN networks due to having a large bandwidth and a very high data rate of gigabits per second [3,4]. High propagation losses in the mmWave band, especially at 60 GHz (where a strong absorption peak occurs due to resonance of oxygen molecules), requires an upgraded infrastructure and new hardware concepts, and the use of fixed beam antenna or omnidirectional antenna will no longer be useful. To overcome these problems, several studies have recently been conducted using multi-beam antennas for increasing signal in the desired direction while rejecting the interfering signals thereby enhancing capacity and quality of service [5]. These antennas can be divided into two categories: adaptive

^{*} Corresponding Author

antenna and switched beam antenna. Switched beam antennas consist of an array connected to a BFN. Among the different BFNs, BM has attracted a lot of attention due to its smaller number of components, lower loss, and ability to produce orthogonal beams [6]. The BM as a passive feeding network for the antenna array provides a uniform amplitude distribution as well as a constant phase difference between the array elements. The components of the BM are: 90° or 3 dB hybrid coupler, 0 dB crossover, and fixed phase shifters.

The BM network has N inputs and N outputs, which can generate N orthogonal beams $(N=2^n \ \forall \ n=1,2,...)$. BM performs the analog signal processing identical to a spatial Fast Fourier Transform (FFT) which greatly simplify the beamforming circuit by replacing a large number of power dividers $(N^*(N-1))$ with a smaller matrix of hybrid couplers $(\frac{N}{2}*\log_2 N)$ [7].

Concisely, at frequencies below 10 GHz due to the large electrical size, researchers have focused their study on the physical dimensions of BMs and tried to compact this circuit as much as possible. At higher frequencies, the physical size is innately decreased, whereas the propagation loss is inevitably increased. Therefore, power losses at mmWave frequencies are the highest concern and include the most important design considerations. Consequently, BMs are implemented in a simple and effective structure and on low-loss substrates. The SIW transmission line with having the advantages of low loss, high-Q factor, high power capacity, and excellent integration capability, is widely used in mmWave BM designs [8-11]. These articles present a 4×4 BM respectively by using SIW short-slot couplers [8, 9], or in a very compact configuration [10], or with two-dimensional beam steering capability [11].

As stated before, a classic BM is an $N \times N$ network to generate uniform amplitude and linear phase distribution. Based on phased array theory [12], the SLL of the uniformly illuminated linear array is about -13 dB. Considering the mutual coupling and the illumination error, the realized SLL is approximately – 9 dB. In order to diminish interference, it is important to decrease the amount of SLL. One operational technique for SLL reduction is to adopt tapered amplitude distribution [13, 14]. Accordingly, the modified BMs $2^n \times 2^{n+1}$ are introduced and among them, 4×8 types are mostly used in designs [15]. However, this type is much more complex and bulkier than conventional 4×4 networks, hence, its simplification and downsizing are very important. In this paper, for the first time, a 4×8 BM having a simple, single layer, and low loss structure at 60 GHz is designed and simulated using the SIW transmission line. The simulations are performed in the computer simulation technology (CST) microwave studio which is based on the Finite Integration Technique (FIT). The BM shows excellent characteristics and also it has a very compact size by eliminating several crossovers and using a special type of straight-line phase shifter without using curved lines. So far, designers have relied on a curved line as a phase shifter in their BM designs, which required a deviation from the main transmission line and then back to it, which greatly increased the circuit's area.

The design procedure begins with the analysis and simulation of the components of the BM in Section II, then all these components are integrated, and first, the formation of a 4×4 network is discussed in Section III, Finally, the design of the overall structure of the 4×8 network ends with the addition of power dividers, crossovers, and straight-line phase shifters in Section IV. To ensure the design validation and verification, simulations are also performed using Ansys HFSS, which is based on finite element method (FEM). The results of these two simulators have an acceptable match.

II. SIW BUTLER MATRIX COMPONENTS

The condition for the beams to be orthogonal in the BM is that there is a progressive phase difference of $\frac{2\pi}{N}$ between the output ports phase differences with excitation of one input port, and the output ports phase differences with excitation of another input port. For instance, in the 4×4 BM of Fig. 1, this phase difference is 90°. For N orthogonal beams, the position of the beam peaks can be expressed as (1) [16].

$$\theta_{peak} = \sin^{-1}\left(\frac{\alpha}{k_0 s}\right) \tag{1}$$

where s is the array element spacing, k_{θ} is the wave number in free space, and α is the phase differences of adjacent outputs. Table 1 shows the progressive phase difference of the outputs as well as the position of the beam peaks for $s=\frac{\lambda_{\theta}}{2}$ where λ_{θ} is free space wavelength.

As shown in Fig. 1, the input signal entered to port 1 passes through the shown path and reaches the output ports with a phase difference of 45° which generates a beam in the position of 14.5°. likewise, if the signal enters port 2, the phase difference will be -135°. The SIW configuration design is developed on a Rogers RT5880 laminate with a thickness of 0.254 mm (10mil) with complex permittivity of ε_r =2.2 and $\tan \delta$ =0.0009 at 10 GHz. The important features of this substrate are a very low dielectric loss and stable

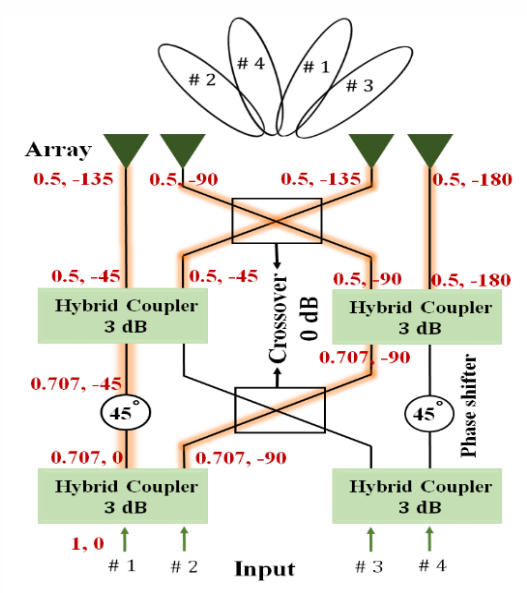


Figure 1. 4×4 BM architecture.

electrical properties with frequency changes. It should be noted that this substrate almost shows the same complex permittivity at 60 GHz [10].

TABLE I. PROGRESSIVE OUTPUT PHASE DIFFERENCES AND THE POSITION OF THE BEAM PEAKS

Input Port	Output phase Differences (a)	Beam Peak Position (θ_{peak})		
1	45°	14.5°		
2	-135°	-48.6°		
3	135°	48.6°		
4	-45°	-14.5°		

In this architecture, the substrate is coated with a layer of electrodeposited copper (thickness $t = 35 \mu m$) on each side. The diameter and pitch of the vias are, respectively, d=0.3 and p=0.6 mm.

Since SIW has discontinuous sidewalls created by vias, it cannot support TM modes and only TE modes can exist [17]. Therefore, the dominant propagating mode in an SIW is $TE_{mn}=TE_{10}$ mode (m=1, n=0). For an SIW, the equations for an ideal rigid waveguide need to be adjusted slightly. [17] has focused on finding effective dimensions of an SIW. An empirical equation is presented in [17] that takes into account the SIW width, w_{siw} , as well as via diameter, d, and spacing, p, and the effective width, w_{eff} of the SIW:

$$w_{eff} = w_{siw} - 1.08 \frac{d^2}{p} + 0.1 \frac{d^2}{w_{siw}}$$
 (2)

Selecting f_c =41.9 GHz for TE₁₀ mode cutoff frequency yields an operation frequency of f_{op} =60 GHz (143% of f_c). For the chosen cutoff frequency, the dielectric filled waveguide's equivalent width should be w_{eff} =2.41 mm and according to (2), this leads to the SIW width of w_{siw} =2.57 mm.

A. 3 dB Hybrid Coupler

The 4-port hybrid coupler, as seen in Fig. 2, is one of the most important components of the BM, which has two very significant features: first) when power is applied to port 1 it is equally distributed in ports 2 and 3, and port 4 is isolated since no power reaches it, second) There is a 90° phase difference between port 2 and port 3 ($\angle S_{21}$ - $\angle S_{31}$ or $\angle S_{24}$ - $\angle S_{34}$). It can be shown that the hybrid coupler's S matrix will have the following form [18]:

$$\mathbf{S} = \frac{-1}{\sqrt{2}} \begin{bmatrix} 0 & \mathbf{j} & 1 & 0 \\ \mathbf{j} & 0 & 0 & 1 \\ 1 & 0 & 0 & \mathbf{j} \\ 0 & 1 & \mathbf{j} & 0 \end{bmatrix}$$
 (3)

Through Even-Odd mode analysis and by taking advantage of the reflection cancellation effect technique [8, 9], the slot length (l) and width (w) design equations for this coupler, which is a short slot coupler, can be derived. Then, the explicit design equations for the slot width and length are given as (4) and (5).

Therefore, if we adopt $|S_{31}| = \frac{1}{\sqrt{2}}$, (4) and (5) will be as:

$$w = \frac{\pi}{k} \sqrt{\frac{4(3n+1)(n+1)}{4n+1}}$$
 (6)

$$l = \frac{\pi}{k} \sqrt{\frac{(3n+1)(n+1)}{3}} \tag{7}$$

where k is the wavenumber and n is a non-negative integer.

By adopting n=1, to have a smaller dimension, the calculated results are w=4.26 mm and l=2.75 mm.

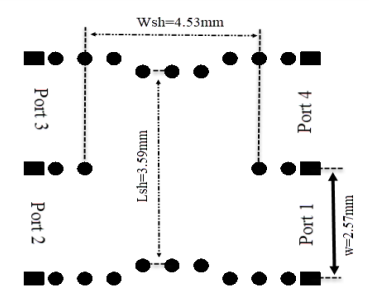


Figure 2. Hybrid coupler's design parameters

Fig. 3 shows the electric field distribution, where the power from the input port is halved on both output ports and port 4 is isolated. Simulated S-parameters of the hybrid coupler are plotted in Fig. 4. The simulation results display the good performance of this coupler. Within the desired frequency range of 57-63 GHz, the return loss level for all ports is lower than 25 dB, and ports 2 and 3 depict insertion loss (IL) of 3.3 dB and 3.1 dB respectively at the operation frequency. The phase difference between port 2 and port 3 of the structure is around 89.8° across the frequency range, which indicates the excellent wideband performance of the hybrid coupler.

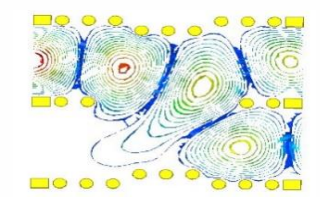
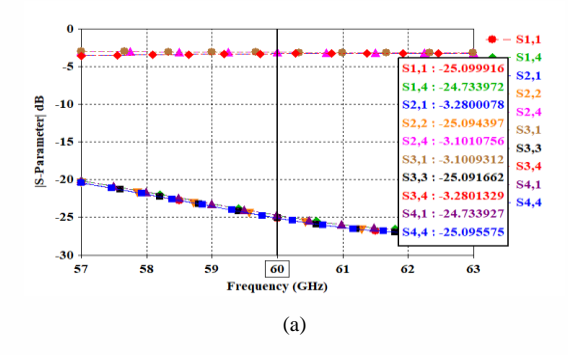


Figure 3. Hybrid coupler's electric field distribution.



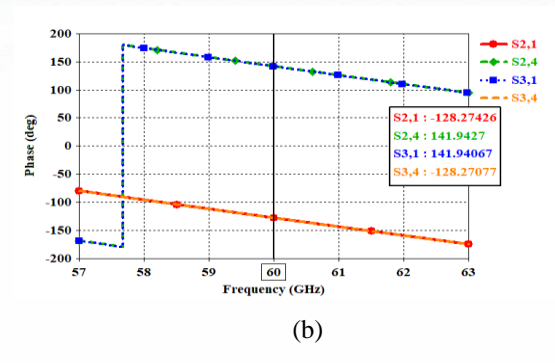


Figure 4. Simulated S-parameters of the hybrid coupler, (a) reflection, transmission, isolation coefficients, (b) outputs phase.

B. Crossover (0 dB)

The crossover makes it possible to move from one transmission line to another and establishes high insulation between the lines. The perfect design of crossover is accomplished if all adjacent ports are isolated, and as illustrated in Fig. 5, the signal can only pass through one path. Crossover can also be designed by performing Even-Odd mode analysis. A crossover can be formed by cascading two hybrid couplers and its S-parameter matrix is given as [18]:

$$\mathbf{S} = \begin{bmatrix} 0 & 0 & \mathbf{j} & 0 \\ 0 & 0 & 0 & \mathbf{j} \\ \mathbf{j} & 0 & 0 & 0 \\ 0 & \mathbf{j} & 0 & 0 \end{bmatrix} \tag{8}$$

with assigning $|S_{31}|=1$, in (4) and (5), equations for slot width and length of the crossover are:

$$w = \frac{\pi}{k} \sqrt{\frac{(6n+1)(2n+3)}{8n}}$$
 (9)

$$l = \frac{\pi}{k} \sqrt{\frac{(6n+1)(2n+3)}{12}}$$
 (10)

Considering that the phase delay of a straight-line SIW is given by $\varphi=\beta_{10}l$, where β_{10} is the phase constant of TE_{10} mode. Generally, the crossover length is inherently small at 60 GHz. Besides, if we choose n with a small value, for example n=1, the crossover length becomes very short. Therefore, in this case, it is very difficult to design a straight line phase shifter associated with the crossover with the selected SIW width.

Furthermore, if we consider the 4×8 BM consisting of two parts: first) 4×4 BM and second) power dividers with a number of crossovers, in the first part more area is available, hence, we have more choice over larger dimensions. Therefore, to obtain more accuracy in the output phase differences, the curved line phase shifters

have been selected in the first part since they follow the crossover output phase more accurately and within a larger bandwidth. A longer crossover slot length can make the curved line phase shifters smooth, have a uniform phase shift toward the output phase of the crossover, and eases the design of the phase shifters.

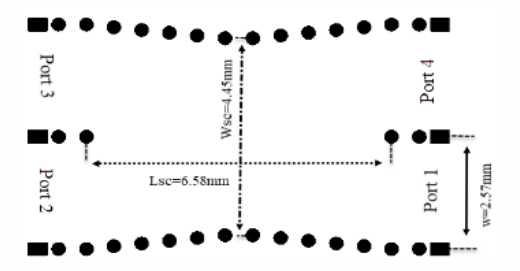
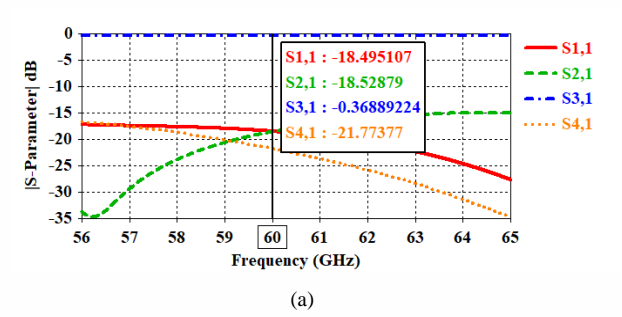


Figure 5. Crossover's design parameters.



Figure 6. Crossover's electric field distribution.



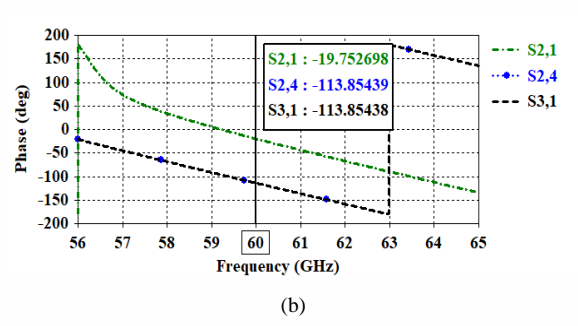


Figure 7. Simulated S-parameters of the crossover, (a) reflection, transmission, isolation coefficients, (b) outputs phase.

Consequently, n=3 is adopted to start the design and the optimal values of Fig. 6 are w=4.45 mm and l=6.58 mm . Fig. 7 illustrates the simulated S-parameters of the crossover with the optimized design parameters. The results show a good performance in

$$w = \frac{\pi}{k} \sqrt{\frac{\left[\pi(2n+2) + 4\sin^{-1}|S_{31}|\right] \left[3\pi(2n+1) - 4\sin^{-1}|S_{31}|\right]}{8\sin^{-1}|S_{31}|\left[\pi(2n+1) + 2\sin^{-1}|S_{31}|\right]}}$$

$$l = \frac{(2n+1)\pi}{2\sqrt{k^2 - (\frac{\pi}{w})^2}}$$
(5)

both signal paths of port 1 to port 3 and port 4 to port 2. Within the frequency range of 56-65 GHz, the return loss is below 18 dB, in addition, S_{31} is nearly constant and is approximate -0.37dB. Isolation levels of more than 18 dB are obtained between port 1 and port 2 (S_{21}) and between port 1 and port 4 (S_{41}). The simulated crossover outputs show a phase of -113.85° at the central frequency.

C. SIW Curved line Phase Shifters of The First Part

Phase shifters make the condition of progressive and sequential output phase differences feasible. They are used to compensate the phase introduced by the crossover as a reference. The circuit requires two 45° phase shifters and two 0° phase shifters. These phases are determined based on the reference phase of the crossover. The phase difference between two transmission lines with different lengths is calculated as follows:

$$\Delta \varphi = \beta_{10} \Delta l$$

$$\beta_{10} = \sqrt{k^2 - k_c^2}$$
(11)

Therefore, for the adopted SIW the value of β_{10} is 424π . According to (11), for the 0° phase shifters, we have:

$$\Delta \varphi = 2\pi \Longrightarrow \Delta l = l_2 - l_1 = 4.7 \text{ mm}$$

Since the length of the crossover was calculated to be l_1 =6.58 mm, then we have l_2 =11.28 mm. According to Fig. 8, l_2 is the length of the arc opposite a line with the length of l_1 (length of crossover) in a circle with radius R.

Point C is on the perpendicular bisector of the line with the length of l_1 . To obtain L_p we can derive:

$$l_{1}=2 R \sin \frac{\theta}{2}$$

$$l_{2}=R \theta$$

$$R=L_{p}+r$$

$$r=R \cos \frac{\theta}{2} \implies L_{p}=R(1-\cos \frac{\theta}{2})$$

$$R=L_{p}+R(1-\cos \frac{\theta}{2})$$

The values of R and $L_{\rm p}$ are calculated as 3.55 mm and 2.24 mm, respectively. $L_{\rm p}$ is the length of the phase shifter curvature and for 0° phase shifters it is optimized to be 2 mm, seen in Fig. 9. Similarly, for 45° phase shifters we have:

$$\Delta \varphi = \frac{9\pi}{4} \Longrightarrow \Delta l = l_2 - l_1 = 5.3 \text{ mm}$$

Consequently, for l_2 =11.88 mm, the values of R and $L_{\rm p}$ are 3.4 mm and 2.43 mm, respectively. After optimization $L_{\rm p}$ becomes 2.3 mm, seen in Fig. 10. Fig. 11 shows the simulated output phases of -158.85 $^{\circ}$ (-113.85 $^{\circ}$ -45 $^{\circ}$) and -113.85 $^{\circ}$ at 60 GHz for 45 $^{\circ}$ phase shifters and 0 $^{\circ}$ phase shifters, respectively.

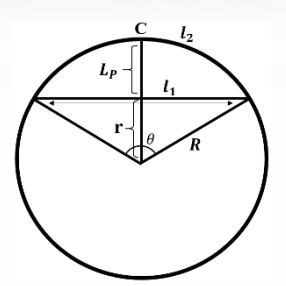


Figure 8. Length of the phase shifters curvatur



Figure 9. The 0° phase shifters.

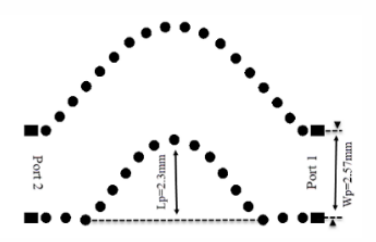


Figure 10. The 45° phase shifters.

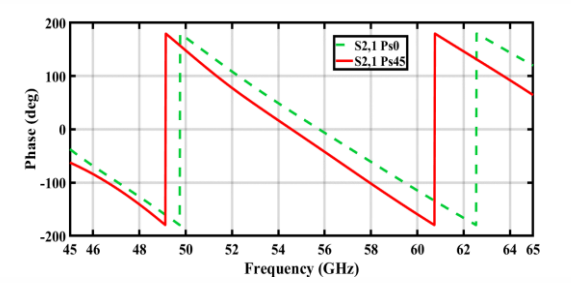


Figure 11. Simulated output phases of phase shifters.

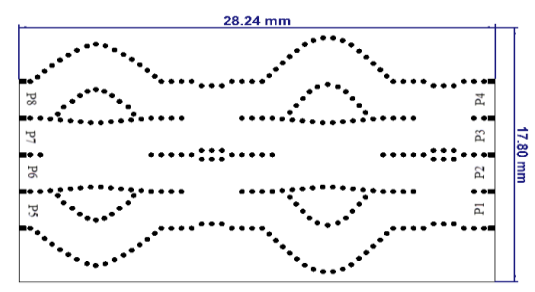


Figure 12. The 4×4 BM.

III. 4×4 BUTLER MATRIX

Finally, the 4×4 BM is realized by integrating all related components, as illustrated in Fig. 12, and its overall size is $28.24 \text{ mm} \times 17.8 \text{ mm} (4\lambda \times 6.3\lambda)$. As inputs are excited, the reflection and coupling levels are less than -10 dB over the frequency range of 55-65 GHz and the insertion loss magnitude imbalance is below 3.1 dB. Fig. 13 illustrates the simulated S-parameters of the BM. Table 2 compares the BM with the simulated BM in articles [10, 11, and 14]. [10] presents a compact 60 GHz SIW 4×4 BM that has a simulated maximum phase error of 41° within the 58-62 GHz, whereas this

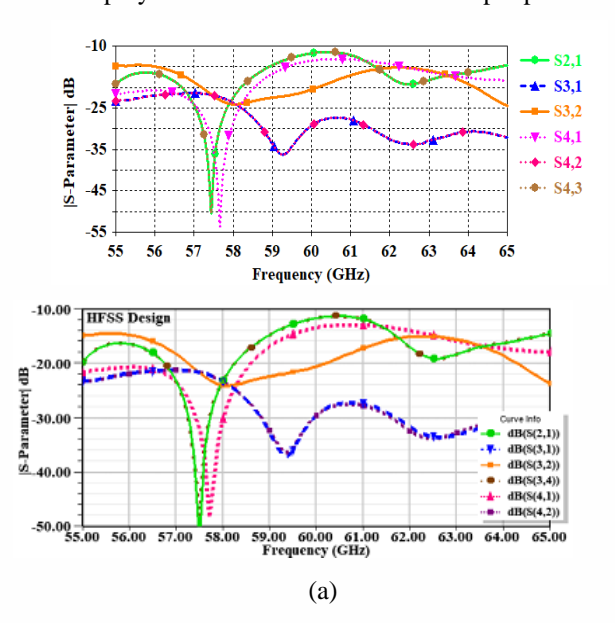
work has a maximum phase deviation of 24.4°. [11] explored a two-dimensional (2-D) beam steering SIW 4×4 BM operating at 60 GHz, which shows a simulated 34.3° peak phase error. Paper [14] developed a ridged waveguide 4×4 BM with side lobe level control in 60 GHz, which has a low insertion loss but results in a more area-consuming BM circuit.

The high accuracy of the designed configuration in this work leads to the correct position of the beams. Generally, in designing a BM, there are three challenges you should face with. First, you should increase the accuracy of the output phase differences, because it results in an accurate beams location and the most important function of a BM is to generate beams in desired locations. Second, The structure compactness must also be considered. Third, an optimal crossing route design should be adopted to minimize the propagation loss, especially at higher frequencies.

The progressive output phase differences are shown in Fig. 14, for input 1 and 2 excitation. Table 3 presents the simulated outputs phase and amplitude and compare them with the ideal values.

IV. 4×8 BUTLER MATRIX

According to the block diagram of Fig. 15, the designed 4×8 BM consists of two parts. The first part includes 4×4 BM and the second part is composed of four T-junction power dividers to establish tapered amplitude distribution, and a series of crossovers to create a proper feeding network. Moreover, corresponding to each of the crossovers and also to compensate the output phase differences of the dividers, one 0° phase shifter must be considered. For instance, the path of the output ports 5 and 12 has four 0° phase shifters. Also, in order to remain the desired phase gradients, several 180° phase shifters are required to be employed in the half number of the output paths.



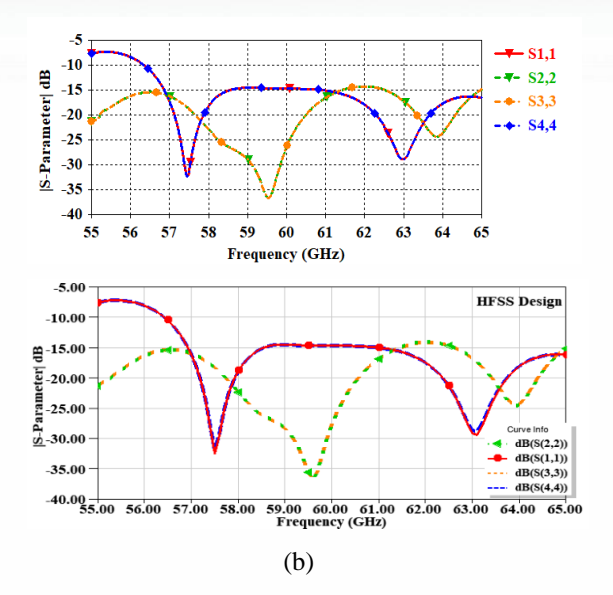


Figure 13. Simulated S-parameters of the 4×4 BM, (a) isolation coefficients (CST & HFSS), (b) reflection coefficients (CST & HFSS).

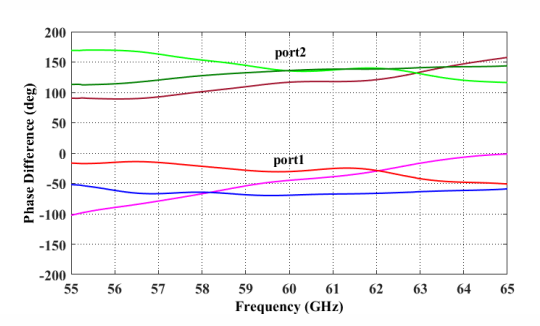


Figure 14. Progressive output phase differences.

To simplify the arrangement and reduce the overall area, the 180° phase shifters have been removed and will be compensated by reversing the antenna elements connected to the 9 to 12 output ports shown with the negative signs. Also, the four 0° phase shifters in the path of the output ports 5 and 12 are merged in one, as the two 0° phase shifters of outputs 6 and 11. In addition, in the second part, instead of using curved line phase shifters, which take up more space due to their curvature, straight-line phase shifters are used that while being straight and short, they can follow the phase delay of crossovers and dividers. Due to employing straight line phase shifters, it is also possible to design crossovers with smaller lengths. Therefore, the value of n in Section II. n is considered as n=2.

Table 4 shows the outputs ideal phase and amplitude. The outputs amplitude ratios of the power dividers are selected according to the distribution of 0.16, 0.361, 0.799, 1, 1, 0.799, 0.361, and 0.16 respectively. According to Fig. 16, two power divider types of D1 and D2 must be designed to obtain the required amplitude distribution.

TABLE II. 4×4 BM SIMULATED OUTPUTS AMPLITUDE.

Input Ports Output Ports	Output Amplitude (dB), Input #1	Output Amplitude (dB), Input #2	Ideal Output Amplitude (dB)	
# 5	-7.2	-8.2	-6	
# 6	-6.3	-7.5	-6	
#7	-9.1	-5.9	-6	
#8	-7.9	-7.2	-6	

TABLE III. Outputs ideal phase and amplitude for 4×8 BM.

Inputs Outputs	#1	#2	#3	#4	Output Amplitude (dB)
# 5	0	0	0	0	-14.62
# 6	-45	135	-135	45	-11.09
# 7	-90	-90	90	90	-7.64
# 8	-135	45	-45	135	6.66
# 9	-180	180	-180	180	6.66
# 10	135	-45	45	-135	7.64
# 11	90	90	-90	-90	11.09
# 12	45	-135	135	-45	14.62

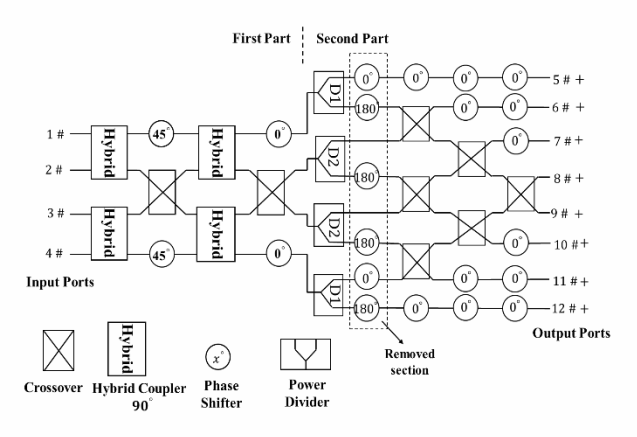


Figure 15. 4×8 BM block diagram.

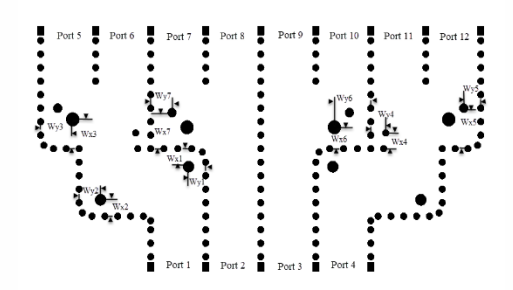


Figure 16. T-junction power dividers design.

All the post positions are optimized for minimizing reflection and getting the right power division ratio. The outputs of D1 and D2 do not need to be in phase, as the following 0° phase shifters can be adjusted to compensate the phase error. Table 5 presents the values of the power dividers design parameters.

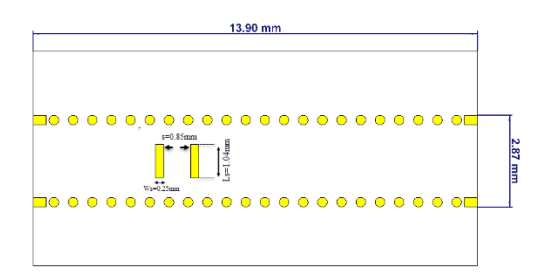


Figure 17. -22° phase shifting with $\angle S_{21} = 10^{\circ}$.

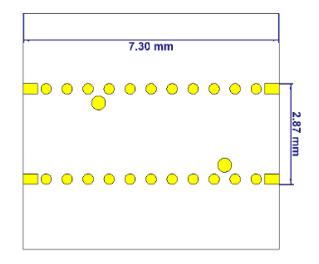


Figure 18. 41° phase shifting with $\angle S_{21} = -145^{\circ}$

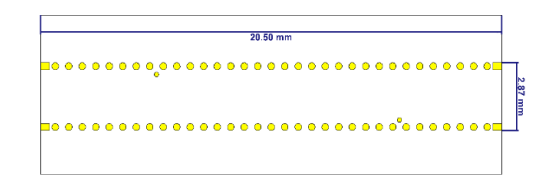


Figure 19. 15° phase shifting with $\angle S_{21} = -92^{\circ}$

TABLE IV. VALUES OF THE POWER DIVIDERS DESIGN PARAMETERS

	Units (mm)							
Wy3	Wy3 Wx3 Wy2 Wx2 Wy1 Wx1 Wy							
1.5	1.3	1	0.3	0.8	0.8	1.7		
Wx6	Wy5	Wx5	Wy4	Wx4	Wy7	Wx7		
0.95	0.8	1.8	0.7	0.7	1	1.6		

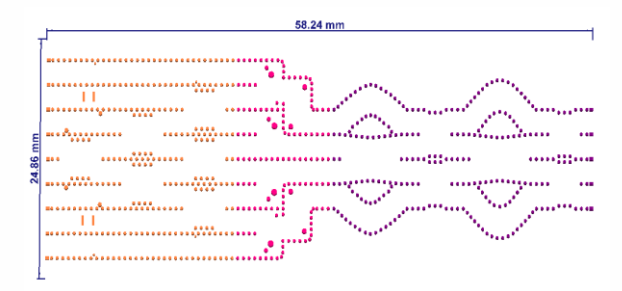


Figure 20. 4×8 BM

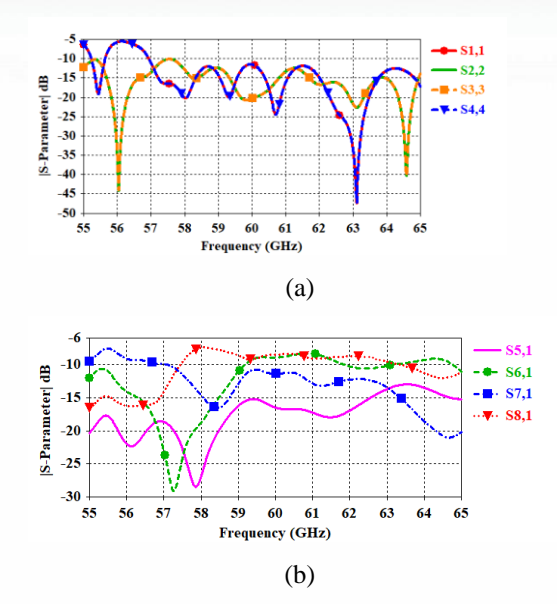


Figure 21. Simulated scattering parameters of the 4×8 BM, (a) reflection and (b) transmission coefficients.

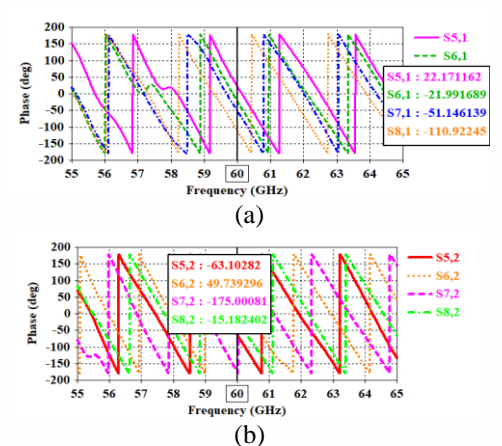


Figure 22. Output phase for inputs (a) 1 and (b) 2 excitation.

Three 0° phase shifters with two design models are used in the second part to create the correct output phase. In the first model, according to [19], apertures in the top or bottom wall of an SIW, as seen in Fig. 17, change the phase constant of the waveguide. The change offers an additional phase lag with respect to an SIW with no slot. Parametric layout simulations show each slot yields a phase shift of 8° to 24° when changing the area of the slot from 0.081 mm² to 0.484 mm². In general, increasing the spacing and area of the rectangular slots had a direct relationship with the magnitude of the phase shift and return loss, and inversely correlated to the insertion loss. With a parametric search of slot dimensions, the desired phase delay is achieved. Two apertures with dimensions of 1.04 mm×0.25 mm and space of 1.1 mm are designed in the top wall. These phase shifters are in the path of the output ports 6 and 11. In the second model, according to [20], two posts as seen in Fig. 18 and Fig. 19, in the path of the output ports 5, 7, 10, and 12, can define an additional phase lead.

By integrating all components, the 4×8 BM is realized, as illustrated in Fig. 20. The ultimate dimensions of the network are 24.86 mm×58.24 mm $(13\lambda \times 5.6\lambda)$, which is in a more compact dimension than previous similar works. The BM indicates high accuracy since it has a maximum phase deviation of 24.8° for excitation of input ports 2 or 3. Simulated scattering parameters are seen in Fig. 21, and the output phases are shown in Fig. 22. Due to the symmetry of BM, the results for excitation of inputs 3 and 4 are not included for brevity, since they have the same signatures. Reflection and isolation coefficients for excitation of all inputs are less than -10 dB within the bandwidth. The relative bandwidth for VSWR<2 is larger than 16.6%. Transmission coefficients show that power is distributed between outputs unequally. Due to similarities, only insertion loss in signal transmission from input 1 to outputs is plotted in Fig. 21. Insertion loss magnitude imbalance is below 2.4 dB. Due to the imbalance, the amplitude distribution of the outputs is different from the ideal values and is associated with an error. Table 6 compares the gradient phase of the outputs with their ideal values.

To assess the BM's SLL suppression performance, a planar slot array antenna fed by the proposed BM is applied, as seen in Fig. 23, and by exciting each input, we evaluate the far-field of the proposed structure. A parametric search on an array factor was conducted to specify the SLL and beam overlap level between adjacent radiated beams as a function of the coupling factors of the couplers. A periodicity of $0.51\lambda_0$ has been considered for the array factor of the final radiating array. By reversing the matching via in this antenna, the removed 180° phase shifters are compensated. Fig. 24 presents the radiation pattern in H-plane for stimulating inputs. The results of the FEM inite Element Method (FEM) which is more accurate for designing antennas while CST is based upon Finite Integration in Technique

The obtained SLL is below -21 dB with the excitation of inputs 1 and 4 and below -14.5 dB for inputs 2 and 3 which is lower than for a classical BM design thanks to the adopted SLL suppression configuration. The half power beam widths are 16.3°, 18°, 18°, and 16.3°, respectively for ports 1, 2, 3, and 4 and the antenna field of view is ±45°. Table 7 compares the designed 4×8 BM with the simulated BM in [13, 14]. [13] presents a modified 4×4 BM at the center frequency of 27.925 GHz, which utilizes two attenuators in two external channels of the BM to realize a tapered amplitude distribution.

It can be observed that the proposed structure exhibits a good performance with having acceptable dimensions compared to similar performed works, wide usable bandwidth, and high accuracy of the beam locations.

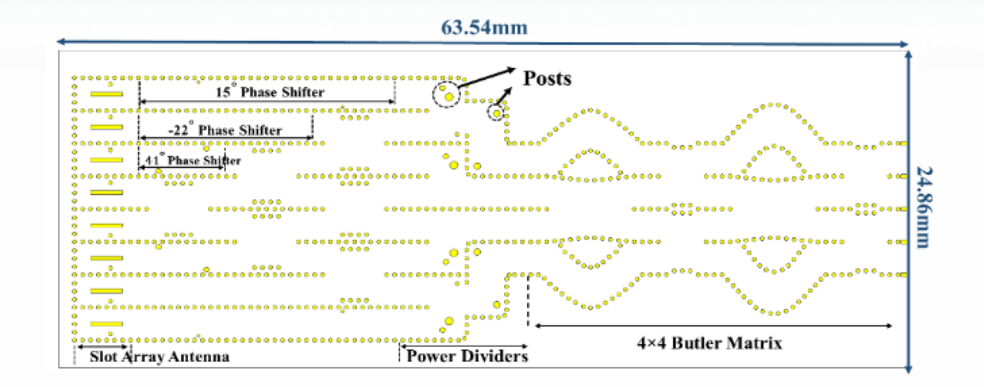


Figure 23. Proposed BM configuration as a feeding network.

TABLE V. COMPARISON OF 4×4 BM WITH THE SIMULATED BMS IN REFERENCE ARTICLES.

Reference	Frequency (GHz)	Technology Type Size		BW (%)	Simulated Phase Error	
[10]	58-62	SIW	4×4	7.23mm×8.8mm	6	41°
[11]	55-65	SIW	4×4	92.21mm×15.10mm	16.6	34.3°
[14]	59-63.5	Ridged waveguide	4×4	70mm×130mm	6.5	_
This Work	56.5-66.5	SIW	4×4	24.28mm×8.17mm	16.6	24.4°

TABLE VI. 4×8 BM OUTPUTS PHASE DIFFERENCES.

Output Ports Input Ports	#6-5	#7-6	#8-7	Phase Difference AVG	Ideal Phase Difference	Maximum Phase Error	Error
#1	-44.17°	-29°	-59.9°	-44.4°	-45°	16°	0.6°
#2	112.73°	135.27°	159.8°	135.9°	+135°	24.8°	0.9°

TABLE VII. COMPARISON OF 4×4 BM WITH THE SIMULATED BMS IN REFERENCE ARTICLES.

Reference	Frequency (GHz)	Technology	Туре	Size	BW (%)	SLL
[14]	59-63.5	Ridged waveguide	4×4	14.35λ×26.65λ	6.5	-17.5 dB
[13]	27.5-28.5	SIW	4×8	6.1λ×4.1λ	3.5	-12 dB
This Work	57-67	SIW	4×8	5.6λ×13λ	16.6	-14.5 dB

V. CONCLUSION

In this article, a 4×8 BM is designed at 60 GHz which in addition to having a simple and low loss structure, has high accuracy and compact dimensions that can be a suitable candidate for new mmWave band technologies such as 5G indoor communication and automotive radar sensing applications. The components were analyzed separately and step by step, based on the requirements of the network. An innovative function was employed to design a straight line SIW phase shifter, using apertures or metal posts to provide the required output phases to diminish the circuit dimensions. All reflection and isolation coefficients are less than -10 dB and the insertion loss is below 2.4 dB within the 57-67 GHz frequency band.

This BM was used as a feed to a slot array antenna with a proper tapered amplitude distribution to assess the SLL improvement. The results showed that this network can reduce the SLL to -21 dB for ports 1 and 4 and -14.5 dB for ports 2 and 3. The four beams radiated can create coverage of 108° at 60 GHz.

REFERENCES

- [1] Chen, Shanzhi, and J. Zhao, "The requirements, challenges, and technologies for 5G of terrestrial mobile telecommunication," *IEEE communications magazine* 52.5 (2014): 36-43.
- [2] W. Roh, J. Y. Seol, J. Park, B. Lee, J. Lee, Y. Kim, J. Cho, K. Cheun, and F. Aryanfar, "Millimeter-wave beamforming as an enabling technology for 5G cellular communications: Theoretical feasibility and prototype results," *IEEE communications magazine* 52.2 (2014): 106-113.
- [3] Tseng, C. Hsiung, C. J. Chen, and T. H. Chu, "A low-cost 60-GHz switched-beam patch antenna array with Butler matrix network," *IEEE Antennas and Wireless Propagation Letters* 7 (2008): 432-435.
- [4] Li, Yujian, J. Wang, and K. Luk, "Millimeter-wave multibeam aperture-coupled magnetoelectric dipole array with planar substrate integrated beamforming network for 5G applications," *IEEE Transactions on Antennas and Propagation* 65.12 (2017): 6422-6431.
- [5] Choi, Junil, Vutha Va, N. Gonzalez-Prelcic, R. Daniels, C.R. Bhat, and R. W. Heath, "Millimeter-wave vehicular communication to support massive automotive sensing," *IEEE Communications Magazine* 54.12 (2016): 160-167.
- [6] Chu, Huy Nam, and Tzyh-Ghuang Ma., "An Extended 4×4 Butler Matrix with Enhanced Beam Controllability and Widened Spatial Coverage," IEEE Transactions on Microwave Theory and Techniques 66.3 (2017): 1301-1311.
- [7] J. Butler and R. Lowe, "Beam-Forming Matrix Simplifies Design of Electronically Scanned Antennas," Electronic Design, vol. 9, no. 4, pp. 170-173, 1961.
- [8] Yamamoto, Shin-ichi, Jiro Hirokawa, and Makoto Ando, "A half-sized post-wall short-slot directional coupler with hollow rectangular holes in a dielectric substrate," *IEICE transactions* on electronics 88.7 (2005): 1387-1394.
- [9] Chen, Chih-Jung, and Tah-Hsiung Chu, "Design of a 60-GHz substrate integrated waveguide Butler matrix—A systematic approach," *IEEE Transactions on Microwave Theory and Techniques* 58.7 (2010): 1724-1733.
- [10] Chen, Zhefan, Xidong Wu, and Fan Yang, "A compact SIW Butler matrix with straight delay lines at 60 GHz," 2017 IEEE International Symposium on Antennas and Propagation & USNC/URSI National Radio Science Meeting. IEEE, 2017.
- [11] Horwath, Benjamin D., and R Abhari, "Characterization of a 4× 4 substrate integrated waveguide Butler matrix at 60 GHz for two-dimensional beam steering." *International Journal of RF and Microwave Computer-Aided Engineering* 28.9 (2018): e21614.

- [12] Mailloux, Robert J, Phased array antenna handbook. Artech house, 2017.
- [13] T. Van, Son, J. M. Lee, Y. Yang, K. Y. Lee, and K. C. Hwang, "A Sidelobe-Reduced, Four-Beam Array Antenna Fed by a Modified 4×4 Butler Matrix for 5G Applications," *IEEE Transactions on Antennas and Propagation* 67.7 (2019): 4528-4536
- [14] Tekkouk, Karim, J. Hirokawa, R. Sauleau, M. Ettorre, M. Sano, and M. Ando, "Dual-layer ridged waveguide slot array fed by a butler matrix with sidelobe control in the 60-GHz band," *IEEE Transactions on Antennas and Propagation* 63.9 (2015): 3857-3867.
- [15] Lian, J. Wei, Y. L. Ban, C. Xiao, and Z. F. Yu, "Compact substrate-integrated 4× 8 Butler matrix with sidelobe suppression for millimeter-wave multibeam application," *IEEE Antennas and Wireless Propagation Letters* 17.5 (2018): 928-932.
- [16] Bhattacharyya, Arun K, "Phased array antennas: Floquet analysis, synthesis, BFNs and active array systems," vol. 179. John Wiley & Sons, 2006.
- [17] F. Xu and K. Wu, "Guided-Wave and Leakage Characteristics of Substrate Integrated Waveguide," IEEE Transactions of Microwave Theory and Techniques, vol. 53, no. 1, pp. 66-73, 2005
- [18] Bhowmik, Wriddhi, and S. Srivastava, "Optimum design of a 4x4 planar butler matrix array for WLAN application," *arXiv* preprint arXiv:1004.4821 (2010).
- [19] Suntives, Asanee, K. Payandehjoo, and R. Abhari, "Design and characterization of periodically-loaded substrate integrated waveguide phase shifters," 2010 IEEE MTT-S International Microwave Symposium. IEEE, 2010.
- [20] Sellal, Kheireddine, L. Talbi, T. Denidni, and J. Lebel, "A new substrate integrated waveguide phase shifter," 2006 European Microwave Conference. IEEE, 2006.



Zahra Mehrzad was born in Shiraz, Iran in 1993. She obtained her B.Sc. in Electrical Engineering from Fasa University in 2016, and the M.Sc. from Amirkabir University of Technology (Tehran Polytechnic), Tehran,

Iran, in 2020. Her research interests are in the areas of Millimeter-Wave and 5G technologies.



Gholamreza Moradi received the Ph.D. degree in Electrical Engineering from Amirkabir University of Technology (Tehran Polytechnic), Tehran, Iran in 2002. His main research interests are numerical Electromagnetics, Antennas, Active Microwave and mm-

Wave Circuits and Systems. He is conducting some collaborative projects on 5G Antenna together with University of Alberta and University of Dresden. Dr. Moradi is currently an Associate Professor with the Electrical Engineering Department, Amirkabir University of Technology. He has published more than one hundred papers in the refereed journals and international conferences. His interests are in the areas

of Antennas, Microwave Imaging, and Millimeter-Wave and 5G technologies.



IJICTR

Ayaz Ghorbani obtained the Postgraduate Diploma, M.Phil., and Ph.D. degrees in Electrical and Communication Engineering and the Ph.D. degree from the University of Bradford, Bradford, UK, in 1984, 1985, 1987, and 2004, respectively.

Since 1987, he has been teaching various courses with the Department of Electrical Engineering, Amirkabir University of Technology, Tehran, Iran. He has authored or co-authored more than 100 papers in various conferences as well as journals. Dr. Ghorbani obtained the John Robertshaw Travel Award and the URSI Young Scientists Award from the General Assembly of URSI, Prague, Czech Republic, in 1990. He was a recipient of the Seventh and Tenth Khwarazmi International Festival Prizes, in 1993 and 1995, respectively, for design and implementation of an Anti-echo Chamber and Microwave Subsystems.